

FBSNet: A Fast Bilateral Symmetrical Network for Real-Time Semantic Segmentation

Guangwei Gao, *Member, IEEE*, Guoan Xu, Juncheng Li, Yi Yu, *Member, IEEE*,
Huimin Lu, *Senior Member, IEEE* and Jian Yang, *Member, IEEE*

Abstract—Real-time semantic segmentation, which can be visually understood as the pixel-level classification task on the input image, currently has broad application prospects, especially in the fast-developing fields of autonomous driving and drone navigation. However, the huge burden of calculation together with redundant parameters are still the obstacles to its technological development. In this paper, we propose a Fast Bilateral Symmetrical Network (FBSNet) to alleviate the above challenges. Specifically, FBSNet employs a symmetrical encoder-decoder structure with two branches, semantic information branch and spatial detail branch. The semantic information branch is the main branch with deep network architecture to acquire the contextual information of the input image and meanwhile acquire sufficient receptive field. While spatial detail branch is shallow and simple network used to establish local dependencies of each pixel for preserving details, which is essential for restoring the original resolution during the decoding phase. Meanwhile, a feature aggregation module (FAM) is designed to effectively combine the output features of the two branches. The experimental results of Cityscapes and CamVid show that the proposed FBSNet can strike a good balance between accuracy and efficiency. Specifically, it obtains 70.9% and 68.9% mIoU along with the inference speed of 90 fps and 120 fps on these two test datasets, respectively, with only 0.62 million parameters on a single RTX 2080Ti GPU.

Index Terms—Semantic segmentation, real-time, feature aggregation, local dependencies.

I. INTRODUCTION

SEMANTIC segmentation, as one of the three fundamental computer vision tasks, is responsible for assigning a label to each pixel in an input image [1]–[3]. It can be viewed as a dense prediction task in that what cannot be avoided is the parameter burden. However, to embed it in real-world terminal equipments like augmented reality devices or autonomous driving chips, it is necessary to ensure that the model size and calculation cost of the proposed model are as small as possible.

G. Gao is with the Institute of Advanced Technology, Nanjing University of Posts and Telecommunications, Nanjing, China, and also with the Digital Content and Media Sciences Research Division, National Institute of Informatics, Tokyo, Japan (e-mail: csggao@gmail.com).

G. Xu is with the College of Automation, Nanjing University of Posts and Telecommunications, Nanjing, China (e-mail: xga_njupt@163.com).

J. Li is with the Center for Mathematical Artificial Intelligence, Department of Mathematics, The Chinese University of Hong Kong, Hong Kong, China (e-mail: cvjunchengli@gmail.com).

Y. Yu is with the Digital Content and Media Sciences Research Division, National Institute of Informatics, Tokyo, Japan (e-mail: yiyu@nii.ac.jp).

Huimin Lu is with the Kyushu Institute of Technology, Kitakyushu 804-8550, Japan (e-mail: dr.huimin.lu@ieee.org).

J. Yang is with the School of Computer Science and Technology, Nanjing University of Science and Technology, Nanjing, China (e-mail: csjyang@njust.edu.cn).

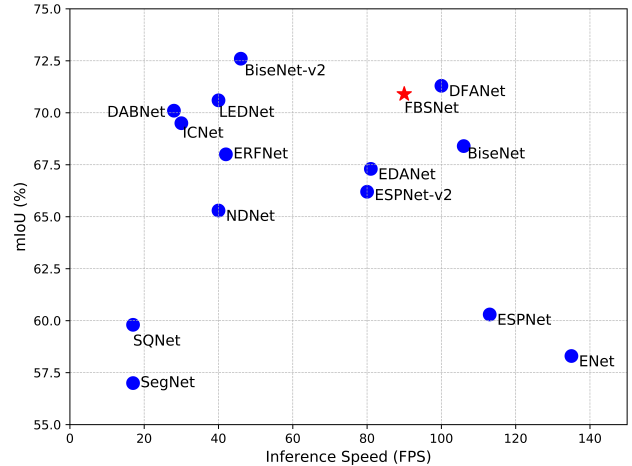


Fig. 1: Accuracy-Speed comparisons on the Cityscapes. The red star represents our FBSNet and the blue dots are other compared methods.

By contrast with developing large networks (e.g., VGGNet [4] and ResNet [5], [6]) that pursue precision, designing real-time semantic segmentation structures is the proper choice that meets the needs of current real-world edge applications requiring fast interaction speed.

Recently, many lightweight real-time segmentation networks have been proposed to address the balance problem between accuracy and inference (Fig. 1). For example, Paszke et al. [7] proposed the efficient neural network (ENet), which drops the last stage to achieve a compact encoder-decoder framework. However, The downside of this model is that the receptive field is too small to capture large objects. For collecting multi-scale contextual information, the efficient spatial pyramid network (ESPNet [8]) adopts an efficient spatial pyramid module and a strategy of convolution factorization, which promotes that the network has similar parameters as ENet, but has better accuracy and inference speed. Image cascade network (ICNet [9]) modified from pyramid scene parsing network (PSPNet [10]), which uses three cascading branches to process images. Nevertheless, this network is not suitable for low-resolution input images. Bilateral segmentation network (BiSeNet [11]) is a dual-path model, which contains two branches and these two branches are used to preserve the spatial details and obtain semantic information, respectively. Meanwhile, a feature fusion module (FFM) was proposed to effectively aggregate the different features of the two branches. Based on BiSeNet, the fusion method of different features

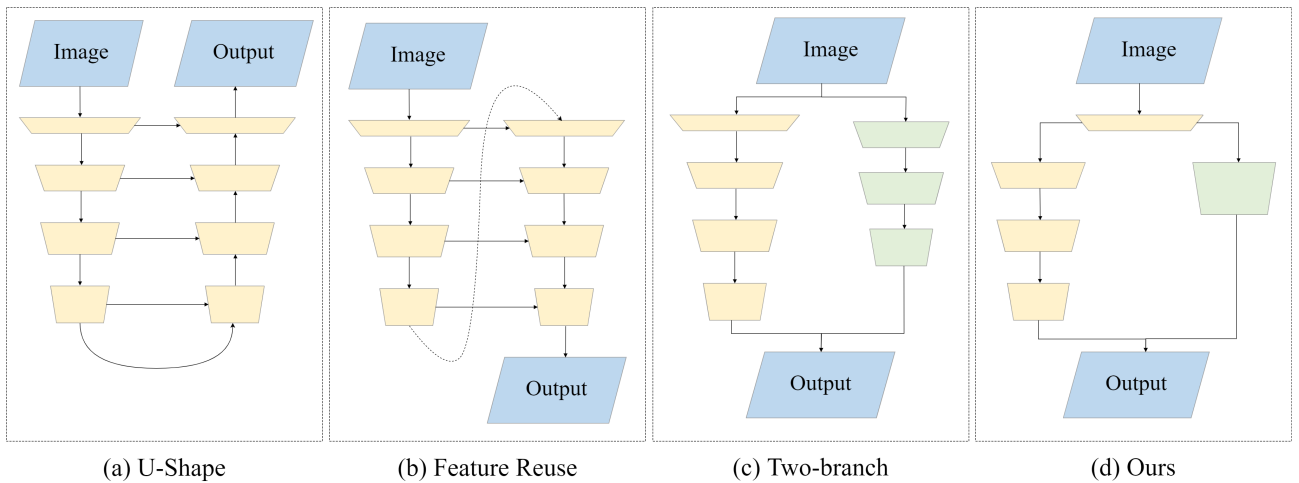


Fig. 2: Structural comparison of common image semantic segmentation models.

in BiSeNet-v2 [12] is further optimized. Although the effect of BiSeNet-v2 is much better than BiSeNet, the number of parameters and calculations has increased a lot, which slows down the inference speed. DFANet [13] proposed a feature reuse strategy, which stacks Xception [14] models three times to yield the purpose of expanding the receptive field and the interactive integration of features. However, due to the deep network layers, the image resolution is down-sampled to a very low level, a lot of boundary information is lost and cannot be recovered. While these works have made impressive achievements, there is still the possibility of improvement in terms of accuracy and speed.

Based on the above observations and considerations, we propose a novel real-time network called Fast Bilateral Symmetrical Network (FBSNet), which is designed for effective inference including higher accuracy and faster speed. FBSNet adopts a bilateral symmetrical encoder-decoder structure, including a semantic information branch and a spatial detail branch. To reduce the weight of the model, we do not use pre-trained models like ResNet [5] or VGG [4] as the backbone in the semantic information branch, but stack our own lightweight modules, named bottleneck residual unit (BRU). BRU employs dilated factorized depth-wise separable convolutional layers to deepen the depth of the network and guarantees large receptive fields for extracting features, and obtaining abundant contextual information. Meanwhile, the spatial detail branch (SDB) makes an effort to preserve spatial details at a small computational cost with a detail residual module (DRM). Moreover, at different stages of the semantic information branch (SIB), we use the channel attention module (CAM) to enhance the long-distance dependencies between channels. Because in the encoder stage of the deep network, most of the image semantic information is contained in the channels, which is why the deeper the network, the more channels there are. Correspondingly, to make up for the lost detailed information in SIB, we use the spatial attention module (SAM) to generate an attention map for paying attention to the useful spatial information and ignoring useless information like noise in SDB. At the end of the two branches, we apply

a feature aggregation module (FAM) to combine and enhance the features at the semantic level and the spatial level. As shown in Fig. 1, FBSNet obtains a good trade-off between accuracy and inference speed with a smaller model size.

In summary, the contributions of this paper are as follow:

- The lightweight bottleneck residual unit (BRU) is proposed to drastically distill significant semantic information. BRU contains a small number of parameters and only need less calculation cost, but can extract rich features with different receptive fields.
- The detail residual module (DRM) is proposed to better obtain shallow spatial features to supplement the details lost in the semantic branch. Meanwhile, the feature aggregation module (FAM) is also proposed to effectively fuse image features from different branches, with the goal to increase the global and local dependencies.
- We present a novel Fast Bilateral Symmetrical Network (FBSNet) for real-time image semantic segmentation task. FBSNet is a symmetrical encoder-decoder structure, composed of a semantic information branch (SIB) and a spatial detail branch (SDB), which can effectively extract deep semantic information and preserve shallow boundary details, respectively.

II. RELATED WORK

A. General Structure

In the past 10 years, many researchers have made a lot of efforts in network structure. Recently, many models still use the network structure of image classification (e.g., VGGNet [4], ResNet [5]) as the model backbone. However, two problems are discovered when we directly use this type of structure: one is that this type of model has too many parameters and the model size is too large, the other is that multiple uses of down-sampling operations will cause a lot of feature loss, which is not conducive to feature discrimination. To solve these problems, some representative network structures came into being, and many subsequent networks are improved based on previous methods, such as U-shape structure [15], [16], feature reuse [13], [17] and two-branch structure [11], [12], [18]. In

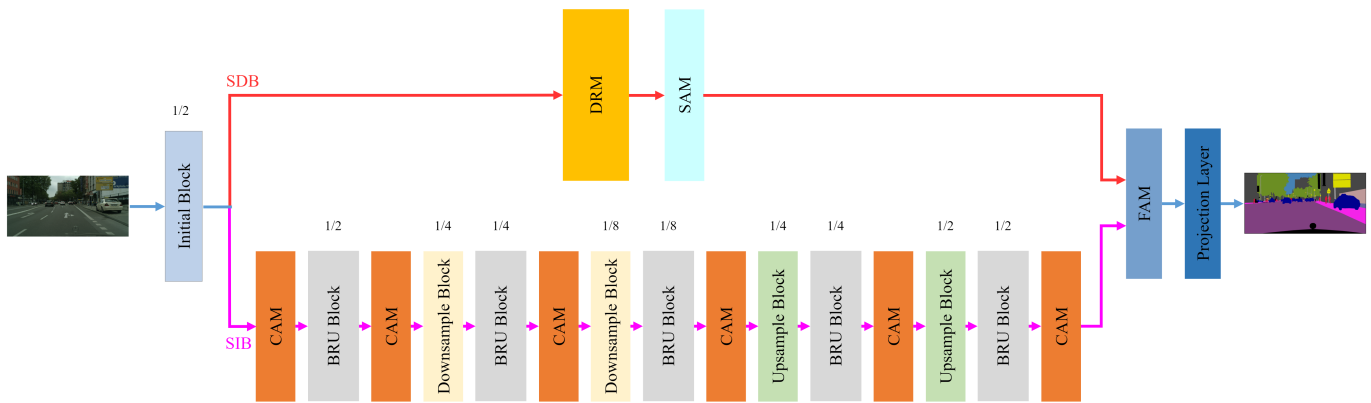


Fig. 3: The complete architecture of our proposed Fast Bilateral Symmetrical Network (FBSNet).

Fig. 2, we provide some structural comparison of common image semantic segmentation models. Among them, the U-shape structure used the symmetrical encoder-decoder, whose strategy is to merge the feature maps of the corresponding stages. However, this kind of network is bound to bring huge additional computation. Feature reuse can enhance the network learning capacity and expand receptive fields by reusing high-level features. However, refining the spatial details is what prevents it from going further. Two-branch structure, separate extraction of semantic information and spatial information, and finally use a feature fusion method before prediction. But this method still lacks the interaction between the two branches, so there is still a lot of room for improvement.

B. Contextual Information

Contextual information is crucial in the field of deep learning-based image processing methods. It contains a large number of image features that can be used for subsequent tasks like classification, detection, segmentation, and other tasks to predict high-quality results [19]–[23].

For example, ParseNet [17] utilized global average pooling to generate weight feature maps for enhancing contextual information. Methods like [24]–[26] employed atrous convolution with various dilation rates to capture diversified contextual information. PSPNet [10], inspired from DeepLab-v3 [26], applied spatial pyramid pooling (SPP) to grab global contexts. DFN [27] encoded the global context by adding the global pooling on the head of the U-shape structure. Based on the above observations, it can be found that increasing the receptive field and acquiring a larger range of global contextual information is what every method cares about, and it is also beneficial to the final segmentation results.

C. Spatial Information

Spatial information is often ignored in the segmentation task. One is that with the deepening of the network layer and the use of consecutive down-sampling modules, the loss of spatial information is considered normal and unavoidable. The other is that restoring spatial information is a difficult task. It often consumes a certain amount of computing resources, so many methods ignore it [28]–[30]. In fact, the preservation

of spatial details has a positive effect on the prediction of the final results. Common methods, such as UNet [15], directly concatenate the shallow details and the features with corresponding resolutions. This operation explicitly claims a large number of parameters and calculations, which is not good for inference speed. In order to supplement the spatial detail information, DABNet [31] inserted features after different multiples of downsampling at different stages in the phase of the encoder. ICNet [9] applied a cascading method to supplement the missing boundary information. Some models [24], [26] adopted dense connections, which cannot fulfill the real-time requirement. These are effective methods, but the decoder lacks semantic guidance, so the final effects will still be slightly worse.

III. PROPOSED METHOD

In this part, we will introduce the network structure of the proposed FBSNet with the following parts: 1) Bottleneck residual unit (BRU); 2) Semantic information branch with channel attention module; 3) Spatial detail branch with spatial attention module; 4) Network with initial block and feature aggregation module.

A. Bottleneck Residual Unit (BRU)

In the semantic information branch, we elaborately design a lightweight bottleneck residual unit. Some classic residual units are shown in Fig. 4, where the two modules in (a) and (b) can not extract semantic information comprehensively, and the pyramid cascade module in (c) requires too much computational cost. To address these problems, we absorb the advantages of the bottleneck, which can not only ensure the model effect but also greatly reduce the calculation budget. Meanwhile, the convolution factorization strategy also be adopted, which means that a standard 2-dimensional convolution kernel $K \times K$ is factored into two 1-dimensional convolution kernels, i.e., $1 \times K$ and $K \times 1$ followed by the batch normalization [33] and ReLU [34] operations. This strategy has been verified in many previous works such as Inception-v3 [35], Xception [14], MobileNet [32], [36], and ShuffleNet [37], [38], which can significantly reduce the model parameters while maintaining the model performance.

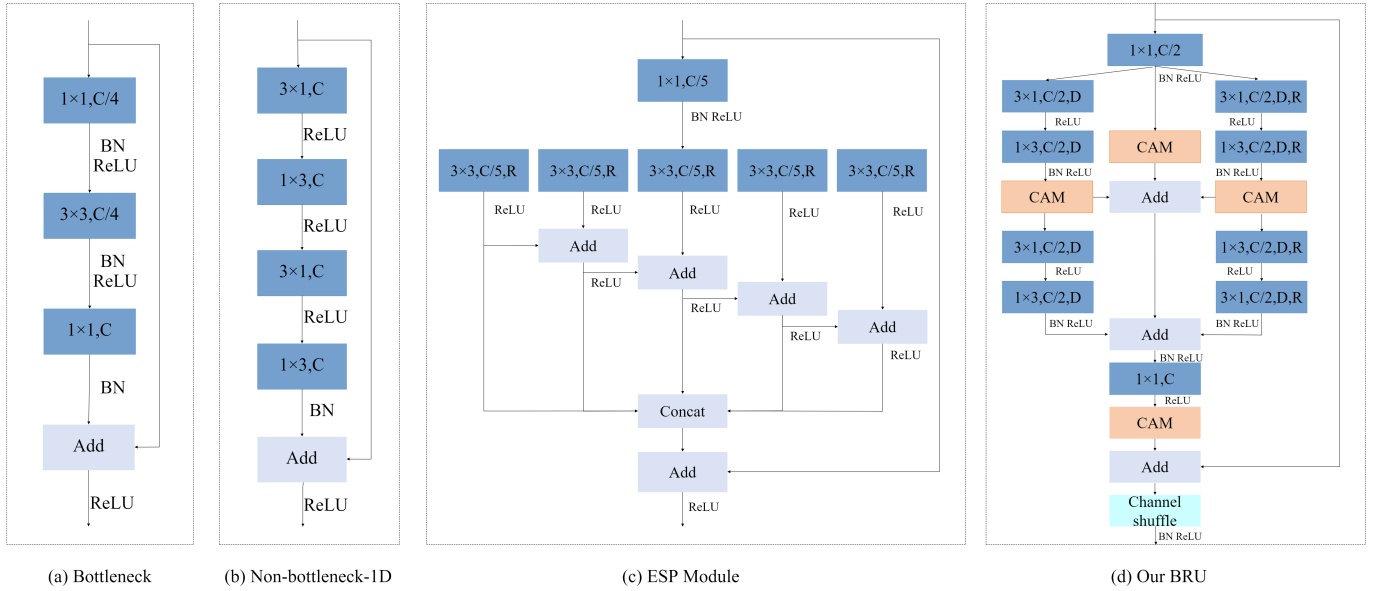


Fig. 4: Comparison of different residual modules. (a) Bottleneck in ENet [7] and MobileNet [32], (b) Non-bottleneck-1D in ERFNet [28], (c) Pyramid cascade module in ESPNet [8], and (d) is our proposed bottleneck residual unit (BRU). “R”: dilation rate, “C”: output channels, and “D”: depth-wise separable convolution.

The use of depth-wise separable convolution is based on the same reason and a 1×1 point-wise convolution is used to recover the final channel dependency. Dilation convolution is applied for enlarging the receptive fields. The rule is that as the network deepens, the dilation rate gradually becomes larger. We employ a channel shuffle operation to enhance the module representation capability, which can further integrate different information after the simple feature fusion operation (addition). As shown in Fig. 4, the whole module is composed of three branches. The left branch is responsible for extracting local and short-distance feature information, the right branch is designed for enlarging the receptive field to acquire long-distance feature information, and the middle branch is dedicated to saving input information. Finally, the information from the three branches is merged together. The formulas of the module can be defined as follows:

$$x_{out} = C_{1 \times 1}(x_{in}), \quad (1)$$

$$y_{1,1} = A(C_{1 \times 3}(C_{3 \times 1}(x_{out}))), \quad (2)$$

$$y_1 = C_{1 \times 3}(C_{3 \times 1}(y_{1,1})), \quad (3)$$

$$y_{2,1} = A(C_{1 \times 3,r}(C_{3 \times 1,r}(x_{out}))), \quad (4)$$

$$y_2 = C_{3 \times 1,r}(C_{1 \times 3,r}(y_{2,1})), \quad (5)$$

$$y_3 = y_{1,1} + A(x_{out}) + y_{2,1}, \quad (6)$$

$$y_{out} = Shuffle(A(C_{1 \times 1}(y_1 + y_2 + y_3)) + x_{in}), \quad (7)$$

where x_{in} and y_{out} mean the input and output of the BRU, respectively. y_1 , y_2 , and y_3 represent the output of the left, right, and middle branch, respectively. The first half of the outputs are represented by $y_{1,1}$ and $y_{2,1}$. Meanwhile, A denotes CAM operation, $C_{m \times n}$ denotes $m \times n$ convolution, r is the dilation rate, and $Shuffle$ is the channel shuffle

operation. The activation function and batch normalization operations are omitted in the formulas.

B. Semantic Information Branch (SIB)

Some modern approaches attempt to obtain sufficient receptive fields and enough contextual information by applying atrous spatial pyramid pooling, large kernel, or dense connection [10], [24], [26]. Although complex networks can occasionally bring good accuracy, the complex calculations make them incompatible with real-time requirements in real-world applications. The dual-branch structure network proposed by BiSeNet [11] used ResNet [5] as the backbone to extract contextual information. The disadvantage is that it occupies too much memory, and the network containing the ResNet [5], which is pre-trained by ImageNet [39] dataset, cannot be regarded as the complete end-to-end learning model. Different from previous works, we build the deep semantic information branch with our proposed BRU. This not only ensures that more semantic information can be captured and larger receptive fields can be obtained, but also that the number of parameters and calculations is very low. Different stages of the convolutional neural networks have different representation abilities: the shallow stages preserve abundant spatial information, such as edges and corners but poor contextual information; while the deep stages have enough semantic consistency but a coarse prediction. According to the above observations, we set different dilation convolution rates in BRU at different stages of the model.

Channel Attention Module (CAM). Since the channels contain abundant feature information and interference noise, we use the channel attention module (CAM) in both BRU and the semantic information branch to emphasize the features that need to be highlighted. Meanwhile, we try to suppress

or ignore the noise. Although CBAM [40], Non-local [41], DANet [42], and CCNet [43] can bring good results, they are potentially not suitable for real-time segmentation tasks due to their complicated calculations and too many parameters. We choose to use the lightweight attention method. CAM uses global average pooling to obtain global contexts and generates an attention map to guide the feature extraction with negligible computation cost, which is a good way to improve the model performance. This method has been generally explored in the tasks of detection, recognition, and segmentation. The process can be given as

$$M_c(X) = \sigma(C_{k \times k}(Trans(AvgPool(X)))), \quad (8)$$

where $M_c \in \mathbb{R}^{C \times 1 \times 1}$ is the desired channel attention map, $X \in \mathbb{R}^{C \times H \times W}$ are the input features, $C_{k \times k}$ represents a standard convolution operation with kernel size k , $Trans$ denote compression and re-weighting operations, and σ is the Sigmoid function.

Downsample Block. Inspired by the initial block in ENet [7], we adopt it as our downsample block. Through the downsampling operation, we can achieve larger receptive fields. However, too many downsampling operations will make the boundary details loss too serious to be restored. Therefore, we take a compromised strategy and only use the downsampling module twice. That is, downsampling it to 1/2 of the input feature each time with the downsample block. So we downsample the image to 1/8 of the original given size eventually.

C. Spatial Detail Branch (SDB)

Spatial information will be inevitably lost in the process of semantic information branch forward derivation. The reason is that the extraction of deep-level semantic information and the preservation of shallow-level boundary information are a pair of contradictory relationships. To solve this problem, we design the spatial detail branch, which is actually a supplement to the detailed information lost by the semantic information branch, to achieve better performance in the final prediction. Different from SIB, we only use a simple and effective detail residual module (DRM, as depicted in Fig. 5 (a)), a spatial attention module (SAM) in this branch. Among them, DRM is stacked by three 3×3 convolutional layers and a 1×1 point-wise convolutional layer, SAM is used to extract and preserve the shallow spatial information of the entire model. To lessen the number of parameters and calculations, we replace the later two convolutions with depth separable convolutions, maintaining the same receptive fields.

Spatial Attention Module (SAM). Different from channel attention focusing on “what”, spatial attention pays more attention to “where”. The practice of spatial attention is to apply both max-pooling and average-pooling along the channel axis, then concatenate and convolve them by a standard convolution to generate an effective feature description. The process of spatial attention is described as follows:

$$M_s(X) = \sigma(C_{k \times k}([AvgPool(X), MaxPool(X)])), \quad (9)$$

where $M_s \in \mathbb{R}^{1 \times H \times W}$ is the desired spatial attention map, $X \in \mathbb{R}^{C \times H \times W}$ are the input features, $C_{k \times k}$ represents a

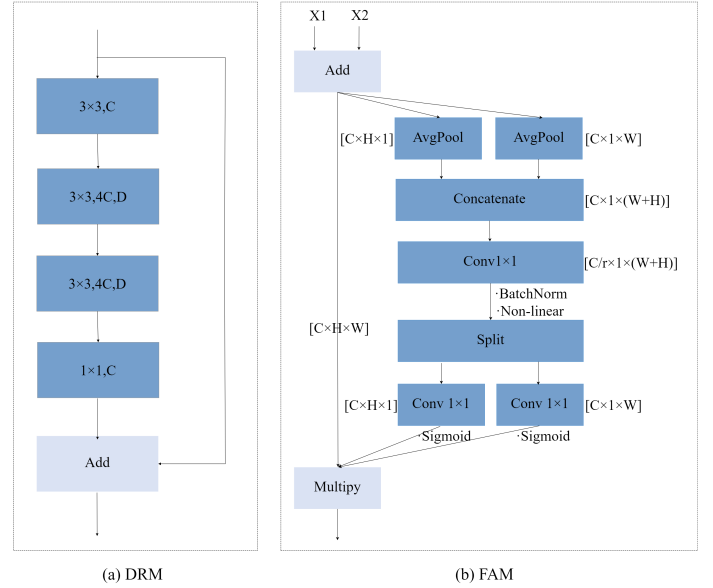


Fig. 5: The complete structure of (a) detail residual module (DRM) and (b) feature aggregation module (FAM).

standard convolutional layer with kernel size k , $[,]$ means concatenation operation, and σ is the Sigmoid function.

D. Fast Bilateral Symmetrical Network (FBSNet)

The whole network structure can be divided into three parts: initial block, dual-branch backbone, and feature aggregation module (the symmetry is mainly reflected in the resolution of the encoding and decoding procedure in SIB). The complete network structure can be found in Fig. 3 and the detailed network structure composition can be found in TABLE I.

Initial Block. The initial block includes three 3×3 convolutional layers, where the stride of the first convolution is set as 2 to collect initial features. If the pooling operation is used, the spatial information will be severely lost. Rather than branching from the original input, where the feature information of the two branches is completely independent [11], [12], the initial block in our method is used as the dividing point of the two branches so that the semantic and spatial information of the two branches are partially correlated, which facilitates subsequent feature merging.

Feature Aggregation Module (FAM). How to effectively integrate the information of the semantic branch and the spatial branch is also the key issue of the two-branch structure. Directly element-wise add or concatenate them are the most widely used methods. However, these methods ignore the differences between the features provided by the two branches. To solve this problem, we used the strategy motivated by the latest attention mechanism [44]. This method can not only capture cross-channel information but also grab information about direction and position perception. The most precious thing is that it is not computation-intensive, which means fewer parameters are in exchange for more gains, especially for dense predictions. Specifically, the global average pooling is factorized into a pair of 1D feature operations.

TABLE I: The detailed architecture of Fast Bilateral Symmetrical Network (FBSNet).

Stage	Layer	Type (Size: $C \times H \times W$)		
Encoder	1	Initial Block	$(16 \times 256 \times 512)$	
	2	CAM	$(16 \times 256 \times 512)$	
	3-5	BRU (d=1) $\times 3$	$(16 \times 256 \times 512)$	
	6	CAM	$(16 \times 256 \times 512)$	
	7	Downsample Block	$(64 \times 128 \times 256)$	
	8-10	BRU (d=1) $\times 3$	$(64 \times 128 \times 256)$	
	11	CAM	$(64 \times 128 \times 256)$	
	12	Downsample Block	$(128 \times 64 \times 128)$	
	13-32	[BRU (d=1) BRU (d=2) BRU (d=5) BRU (d=9) BRU (d=17)] $\times 4$	$(128 \times 64 \times 128)$	DRM $(16 \times 256 \times 512)$ $(64 \times 256 \times 512)$ $(64 \times 256 \times 512)$ $(16 \times 256 \times 512)$
	33	CAM	$(128 \times 64 \times 128)$	SAM $(16 \times 256 \times 512)$
Decoder	34	Upsample Block	$(64 \times 128 \times 256)$	
	35-37	BRU (d=1) $\times 3$	$(64 \times 128 \times 256)$	
	38	CAM	$(64 \times 128 \times 256)$	
	39	Upsample Block	$(16 \times 256 \times 512)$	
	40-42	BRU (d=1) $\times 3$	$(16 \times 256 \times 512)$	
	43	CAM	$(16 \times 256 \times 512)$	
	44	FAM	$(16 \times 256 \times 512)$	
	45	Projection Layer	$(19 \times 512 \times 1024)$	

Given an input $X \in R^{C \times H \times W}$, which is obtained by adding the two output features $X_1 \in R^{C \times H \times W}$, $X_2 \in R^{C \times H \times W}$ from the two branches. Along the horizontal and the vertical coordinate, we employ two spatial pooling kernels with size $(H, 1)$ and $(1, W)$ to encode the features, respectively. After that, we can get two transformations, which respectively merge features along the two spatial dimensions to correspondingly generate attention maps from two directions. One direction is responsible for capturing long-range dependencies, and the other helps to retain precise positional information. For the generated maps, we concatenate them and send them to a shared 1×1 convolutional layer for channel reduction yielding a $C/r \times 1 \times (W + H)$ output. The procedures are formulated as follows:

$$f = C_{1 \times 1} ([AvgPool_h(X), AvgPool_w(X)]), \quad (10)$$

where $[\cdot, \cdot]$ represents the concatenation operation, $AvgPool_h$ and $AvgPool_w$ represent the pooling operation along H and W directions. Batch normalization and non-linear activation function are also used before we split the intermediate features f into two tensors, $f^h \in R^{C/r \times H}$ and $f^w \in R^{C/r \times W}$, respectively. Another two 1×1 convolution operations T_h and T_w are applied to restore f^h and f^w have the same channel numbers as the input X . After passing through two Sigmoid functions, we expand the two outputs and take them as attention weights. The procedures are formulated as follows:

$$K^h = \delta(T_h(f^h)), \quad (11)$$

$$K^w = \delta(T_w(f^w)), \quad (12)$$

Finally, the output Y of the FAM can be calculated as:

$$Y = (X_1 + X_2) \times K^h \times K^w. \quad (13)$$

Through this method, the features of the two branches can be well integrated, and the feature information can be

adaptively highlighted under the channel and spatial directions simultaneously. The complete structure of FAM is provided in Fig. 5 (b).

IV. EXPERIMENTS

In this section, we will introduce the benchmarks datasets we used, the parameter settings during training, the ablation experiments, as well as the comparison with other state-of-the-art image semantic segmentation methods to fully illustrate the advantages of our FBSNet.

A. Datasets

Cityscapes. The Cityscapes dataset records street scenes in 50 different European cities with the size of 2048×1024 , containing 5,000 finely annotated images and 19,998 coarsely annotated images. The dataset involves 30 categories, and we only employ 19 of them with fine-annotated images for training and testing, which is divided into three parts: 2975 samples for training, 500 samples for validation, and 1525 samples for testing.

CamVid. The CamVid dataset is another vehicle applications dataset collected from video sequences. It has 11 categories and 701 finely annotated images that are split into 367 training samples, 101 validation samples, and 233 testing samples with the same size of 960×720 .

B. Implementation details

We implement our model with the PyTorch framework and all our experiments are performed on a single RTX 2080 Ti GPU. For Cityscapes, we train our network from scratch by utilizing cross-entropy loss function with OHEM, as well as the stochastic gradient descent (SGD) method with momentum 0.9 and the related weight decay 1×10^{-4} . As

TABLE II: Ablation studies on CamVid. SIB: Semantic Information Branch, SDB: Spatial Detail Branch, CAM: Channel Attention Module, FAM: Feature Aggregation Module, SAM: Spatial Attention Module.

Models	SIB	SDB	CAM	SAM	Fusion			Parameters (M)↓	FLOPs (G)↓	mIoU (%)↑
					Add	Concatenate	FAM			
(a) CAM										
FBSNet	✓							0.5923	6.74	66.13
FBSNet	✓		✓					0.5923	6.74	66.72
(b) FAM										
FBSNet	✓	✓	✓		✓			0.6148	9.69	67.87
FBSNet	✓	✓	✓			✓		0.6161	9.77	68.26
FBSNet	✓	✓	✓				✓	0.6153	9.69	68.58
(c) SAM										
FBSNet	✓	✓	✓				✓	0.6153	9.69	68.58
FBSNet	✓	✓	✓	✓			✓	0.6154	9.70	68.86

TABLE III: Comparison with state-of-the-arts image semantic segmentation methods on the Cityscapes test dataset. Although our FBSNet did not achieve the best results on mIoU, the model achieves competitive results on the number of parameters, FLOPs, and FPS. In general, FBSNet achieves the best balance between model performance, model size, and inference time.

Methods	Input Size	Backbone	Parameters (M) ↓	FLOPs (G)↓	Speed (FPS)↑	mIoU (%)↑
SegNet [16]	640 × 360	VGG16	29.50	286	17	57.0
ENet [7]	512 × 1024	No	0.36	3.8	135	58.3
SQNet [45]	1024 × 2048	SqueezeNet	-	270.0	17	59.8
ESPNet [8]	512 × 1024	ESPNet	0.36	-	113	60.3
CGNet [23]	360 × 640	No	0.50	6.0	-	64.8
NDNet [46]	1024 × 2048	No	0.50	14.0	40	65.3
ESPNet-v2 [47]	512 × 1024	ESPNet-v2	-	2.7	80	66.2
EDANet [48]	512 × 1024	No	0.68	-	81	67.3
ERFNet [28]	512 × 1024	No	2.10	-	42	68.0
BiseNet [11]	768 × 1536	Xception39	5.80	14.8	106	68.4
ICNet [9]	1024 × 2048	PSPNet50	26.50	28.3	30	69.5
DABNet [31]	1024 × 2048	No	0.76	10.5	28	70.1
LEDNet [30]	512 × 1024	No	0.94	-	40	70.6
DFANet [13]	1024 × 1024	Xception	7.80	3.4	100	71.3
BiseNet-v2 [12]	512 × 1024	No	3.40	55.3	46	72.6
FBSNet (ours)	512 × 1024	No	0.62	9.7	90	70.9

for the CamVid dataset, due to different input resolutions, we adapt the optimization method to Adam with momentum 0.9 and related weight decay 2×10^{-4} . At the same time, to stabilize the training, the ‘poly’ policy is also utilized for the learning rate strategy. The initial learning rate is configured as 4.5×10^{-2} and 1×10^{-3} for Cityscapes and CamVid, respectively, but with the same power 0.9. The learning rate is generally related to the iteration and can be calculated as $lr_{initial} \times \left(1 - \frac{iteration}{max_iteration}\right)^{0.9}$. Both datasets are trained for 1000 epochs with a batch size of 4 for Cityscapes and 6 for CamVid.

C. Ablation Studies

The main purpose of the ablation studies conducted on the CamVid test set is to verify the performance improvement of each module in the entire network. Similar to the controlled variable methods in physics experiments, we add modules step by step to see their impact on the prediction results, the number of parameters, and the amount of computation. All results are provided in TABLE II.

CAM. As we can observe from the first two lines of the data field in TABLE II, the prediction results of the network are worse without using CAM. In other words, the CAM can provide a 0.6% improvement in accuracy with almost no increase in the number of parameters or computation. This experiment fully proves the effectiveness of CAM.

FAM. The feature fusion method has always been the key research topic for multi-semantic aggregation. When referring to the fusion strategy, the ‘‘Add’’ and ‘‘Concatenate’’ operations jump into our minds naturally. Thus, we compare ‘‘Add’’, ‘‘Concatenate’’, and FAM in TABLE II. According to the table, we can observe that FAM gets the best performance of 68.86% and with 1% and 0.6% better than that of the above two fusion strategies, respectively. Compared with the ‘‘Add’’ strategy, FAM only increases negligible parameters and 0.01G FLOPs. Meanwhile, although the accuracy of ‘‘Concatenate’’ is better than that of ‘‘Add’’, it will undoubtedly add unnecessary increases in the calculation burden to the network due to the conversion of channels involved after the concatenation operation.

TABLE IV: Per-class IoU (%) results on the Cityscapes test set.

Methods	Tru	Fen	Wal	Mot	Tra	Pol	Rid	TLi	Ter	Bic	TSi	Bus	Ped	Sid	Bui	Veg	Car	Sky	Roa	Cla
SegNet [16]	38.1	29.0	28.4	35.8	44.1	35.7	42.8	39.8	63.8	51.9	45.1	43.1	62.8	73.2	84.0	87.0	89.3	91.8	96.4	57.0
ENet [7]	36.9	33.2	32.2	38.8	48.1	43.4	38.4	34.1	61.4	55.4	44.0	50.5	65.5	74.2	75.0	88.6	90.6	90.6	96.3	58.3
SQNet [45]	18.8	35.7	31.6	34.0	33.3	50.9	42.6	52.0	65.8	59.9	61.7	41.2	73.8	75.4	87.9	90.9	91.5	93.0	96.9	59.8
ESPNet [8]	38.1	36.1	35.0	41.8	50.1	45.0	40.9	35.6	63.2	57.2	46.3	52.5	67.0	77.5	76.2	90.8	92.3	92.6	97.0	60.3
ESPNet-v2 [47]	53.0	42.1	43.5	44.2	53.2	49.3	53.1	52.6	66.8	59.9	60.0	65.9	72.9	78.6	88.8	90.5	91.8	93.3	97.3	66.2
EDANet [48]	40.9	46.0	42.0	50.4	56.0	52.3	54.3	59.8	68.7	64.0	65.0	58.7	75.7	80.6	89.5	91.4	92.4	93.6	97.8	67.3
ERFNet [28]	50.8	48.0	42.5	47.3	51.8	56.3	57.1	59.8	68.2	61.7	65.3	60.1	76.8	81.0	89.8	91.4	92.8	94.2	97.7	68.0
ICNet [9]	51.3	48.9	43.2	53.6	51.3	61.5	56.1	60.4	68.3	70.5	63.4	72.7	74.6	79.2	89.7	91.5	92.6	93.5	97.1	69.5
DABNet [31]	52.8	50.1	45.5	51.3	56.0	59.3	57.8	63.5	70.1	66.8	67.7	63.7	78.1	82.0	90.6	91.8	93.7	92.8	97.9	70.1
LEDNet [30]	64.4	49.9	47.7	44.4	52.7	62.8	53.7	61.3	61.2	71.6	72.8	64.0	76.2	79.5	91.6	92.6	90.9	94.9	98.1	70.6
FBSNet(ours)	50.5	53.5	50.9	56.2	37.6	62.5	63.8	67.6	70.5	70.1	71.5	56.0	82.5	83.2	91.5	92.7	93.9	94.4	98.0	70.9

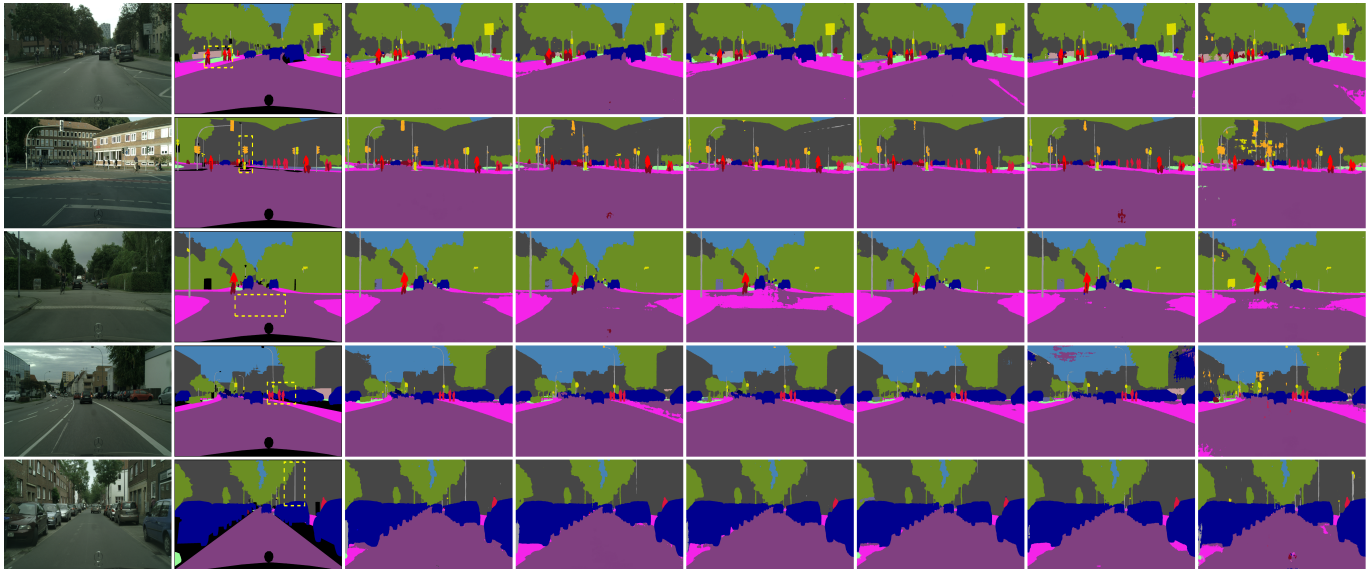


Fig. 6: Sample visual results on the Cityscapes validation set. From left to right: input samples, ground-truth references, segmentation outputs of the proposed FBSNet, LEDNet [30], DABNet [31], ERFNet [28], NDNNet [46], and ENet [7]. The region in the yellow dotted box can intuitively highlight the superiority of our method over others.

SAM. This part is to verify the benefits of SAM in enhancing spatial information. Comparing the last two rows in TABLE II, we can see that SAM can take up only 0.01G of computation and very few parameters, resulting in a performance improvement from 68.58% to 68.86%.

As can be seen from the above three ablation experiments, each module plays a unique role in the network. It can also be found that due to the addition of SDB, the computation of the whole network is increased by nearly a half while the performance is improved from 66.72% to 67.87%. The reason why many methods are reluctant to use it is that their semantic branches are already so computationally heavy that there is no room left to consider the boundary detail information. On the contrary, due to the lightweight structure of our SIB, we can integrate the SIB and SDB to achieve promising performance.

D. Comparison with SOTA Methods

During the training phase, we crop the size of original images and corresponding labels to 1024×512 for Cityscapes and 480×360 for CamVid as input to reduce the computational consumption and the GPU memory occupation. For testing,

we use the original size of the datasets for inference. For a fair comparison, we do not employ any other post-process operations, like conditional random field (CRF). The evaluation indicators of the model are mainly from four aspects: the mean intersection over union (mIoU), the number of parameters, the number of float-point operations (FLOPs), and the inference speed (FPS).

Results on Cityscapes: In TABLE III, we provide a quantitative comparison with other state-of-the-art image semantic segmentation methods on the Cityscapes test dataset. Moreover, we provide the per-class IoU (%) results on the Cityscapes in TABLE IV. According to these tables, we can see that when encountered with fewer parameters, our network can well ensure better accuracy and faster inference speed. The models with the same number of parameters as our method do not have the same effects. The models with the same effects have more number of parameters than ours. Specifically, from the perspective of “Parameters”, ENet [7], ESPNet [8], and NDNNet [46] have fewer parameters but their segmentation accuracy is 5.6% lower than our FBSNet, which is a big gap in the segmentation field. This is in the case that our number

TABLE V: Comparison with state-of-the-arts image semantic segmentation methods on the CamVid test set.

Methods	Input Size	Backbone	Parameters (M)↓	mIoU (%)↑
ENet [7]	360 × 480	No	0.36	51.3
SegNet [16]	360 × 480	VGG16	29.50	55.6
NDNet [46]	360 × 480	No	0.50	57.2
DFANet [13]	720 × 960	Xception	7.80	64.7
Dilation8 [49]	720 × 960	VGG16	140.80	65.3
CGNet [23]	360 × 480	No	0.50	65.6
BiseNet [11]	720 × 960	Xception39	5.80	65.6
DABNet [31]	360 × 480	No	0.76	66.4
ICNet [9]	720 × 960	PSPNet50	26.50	67.1
BiseNet [11]	720 × 960	ResNet18	49.0	68.7
FBSNet (ours)	360 × 480	No	0.62	68.9

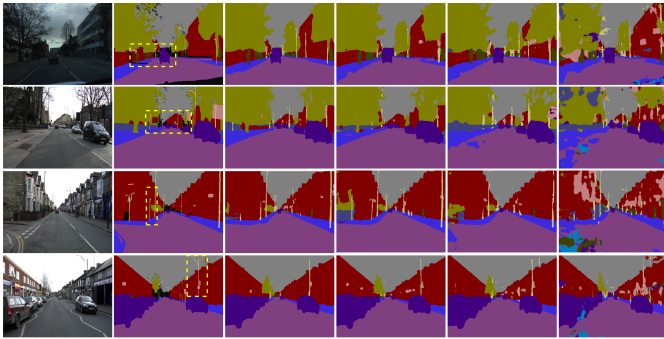


Fig. 7: Sample visual results on the CamVid test set. From left to right: input samples, ground-truth references, segmentation outputs of the proposed FBSNet, DABNet [31], DFANet [13], NDNet [46], and ENet [7]. The region in the yellow dotted box can intuitively highlight the superiority of our method over others.

of parameters is only 0.26M more than theirs. From the perspective of “FLOPs”, the computation cost of ESPNet-v2 [47] is 7G smaller than ours at the cost of 4.7% segmentation performance penalty. From the perspective of “Speed”, our method is in a position above the medium level at 90 FPS. While in terms of “mIoU”, there are only two methods have higher performance than our method, i.e., DFANet [13] and BiseNet-v2 [12]. But they have obviously larger parameters compared with ours. Therefore, we can draw a conclusion that our FBSNet stands out among a number of methods and appear to be very advantageous in balancing accuracy and efficiency. Moreover, we provide the visual comparisons with LEDNet [30], DABNet [31], ERFNet [28], NDNet [46], and ENet [7] in Fig. 6. Through a horizontal comparison of the segmentation results, we can also qualitatively see the advantages of our proposed method. The yellow dotted boxes in the ground truth distinctly depict that our method is obviously superior to other methods.

Results on CamVid: To further verify the performance of FBSNet, we also provide a quantitative comparison with other methods on the CamVid test dataset in TABLE V. For CamVid, under the premise of not using the pre-training strategy, the model size is generally less than 1M. Even though, our method has achieved excellent segmentation re-

sults. According to the table, we can observe that (a) FBSNet achieves the best segmentation results; (b) compared with methods of similar model size, the performance of FBSNet has been significantly improved; (c) compared with other large models, FBSNet achieves better results with fewer parameters. Similarly, we provide the visual comparison results of these methods on the CamVid test dataset in Fig. 7. Obviously, our FBSNet still achieves the best segmentation results. All the above experiments have fully proved the effectiveness and excellence of FBSNet, which strikes a good balance between accuracy and efficiency.

V. CONCLUSIONS

In this paper, we proposed a Fast Bilateral Symmetrical Network (FBSNet) for the real-time image semantic segmentation tasks. Compared to some top-accurate methods struggling for complex architecture and extreme lightweight networks aiming at compressing convolutional layers, our solution mainly focuses on getting a relatively good balance between the accuracy, model size, and inference speed with elaborately designed modules. Especially, our proposed bottleneck residual unit (BRU) can enlarge the receptive field to distill significant semantic information comprehensively. Our extensive investigations have shown that spatial information is critical to recovering the resolution during the decoder process. Therefore, we designed is a symmetrical encoder-decoder model, which composed of a semantic information branch (SIB) and a spatial detail branch (SDB). These two branches can extract deep semantic information and preserve shallow boundary details, respectively. In summary, our network, which is only 0.62M, can process a 1024×512 input size and achieves 70.9% at a speed of 90 FPS on Cityscapes test data with a single RTX 2080Ti GPU. The experiments have revealed that our presented FBSNet can make a better trade-off between accuracy and efficiency.

REFERENCES

- [1] Y. Li, Y. Guo, Y. Kao, and R. He, “Image piece learning for weakly supervised semantic segmentation,” *IEEE Trans. Syst., Man, Cybern., Syst.*, vol. 47, no. 4, pp. 648–659, 2017.
- [2] T. Zhang, G. Lin, J. Cai, T. Shen, C. Shen, and A. C. Kot, “Decoupled spatial neural attention for weakly supervised semantic segmentation,” *IEEE Trans. Multimedia*, vol. 21, no. 11, pp. 2930–2941, 2019.
- [3] G. Gao, G. Xu, Y. Yu, J. Xie, J. Yang, and D. Yue, “Mscfnnet: A lightweight network with multi-scale context fusion for real-time semantic segmentation,” *arXiv preprint arXiv:2103.13044*, 2021.
- [4] K. Simonyan and A. Zisserman, “Very deep convolutional networks for large-scale image recognition,” *arXiv preprint arXiv:1409.1556*, 2014.
- [5] K. He, X. Zhang, S. Ren, and J. Sun, “Deep residual learning for image recognition,” in *Proc. CVPR*, 2016, pp. 770–778.
- [6] C. Szegedy, S. Ioffe, V. Vanhoucke, and A. Alemi, “Inception-v4, inception-resnet and the impact of residual connections on learning,” in *Proc. AAAI*, 2017, pp. 4278–4284.
- [7] A. Paszke, A. Chaurasia, S. Kim, and E. Culurciello, “Enet: A deep neural network architecture for real-time semantic segmentation,” *arXiv preprint arXiv:1606.02147*, 2016.
- [8] S. Mehta, M. Rastegari, A. Caspi, L. Shapiro, and H. Hajishirzi, “Espnet: Efficient spatial pyramid of dilated convolutions for semantic segmentation,” in *Proc. ECCV*, 2018, pp. 552–568.
- [9] H. Zhao, X. Qi, X. Shen, J. Shi, and J. Jia, “Icnet for real-time semantic segmentation on high-resolution images,” in *Proc. ECCV*, 2018, pp. 405–420.
- [10] H. Zhao, J. Shi, X. Qi, X. Wang, and J. Jia, “Pyramid scene parsing network,” in *Proc. CVPR*, 2017, pp. 2881–2890.

- [11] C. Yu, J. Wang, C. Peng, C. Gao, G. Yu, and N. Sang, "Bisenet: Bilateral segmentation network for real-time semantic segmentation," in *Proc. ECCV*, 2018, pp. 325–341.
- [12] C. Yu, C. Gao, J. Wang, G. Yu, C. Shen, and N. Sang, "Bisenet v2: Bilateral network with guided aggregation for real-time semantic segmentation," *arXiv preprint arXiv:2004.02147*, 2020.
- [13] H. Li, P. Xiong, H. Fan, and J. Sun, "Dfanet: Deep feature aggregation for real-time semantic segmentation," in *Proc. CVPR*, 2019, pp. 9522–9531.
- [14] F. Chollet, "Xception: Deep learning with depthwise separable convolutions," in *Proc. CVPR*, 2017, pp. 1251–1258.
- [15] O. Ronneberger, P. Fischer, and T. Brox, "U-net: Convolutional networks for biomedical image segmentation," in *Proc. MICCAI*, 2015, pp. 234–241.
- [16] V. Badrinarayanan, A. Kendall, and R. Cipolla, "Segnet: A deep convolutional encoder-decoder architecture for image segmentation," *IEEE Trans. Pattern Anal. Mach. Intell.*, vol. 39, no. 12, pp. 2481–2495, 2017.
- [17] W. Liu, A. Rabinovich, and A. C. Berg, "Parsenet: Looking wider to see better," *arXiv preprint arXiv:1506.04579*, 2015.
- [18] R. P. Poudel, S. Liwicki, and R. Cipolla, "Fast-scnn: fast semantic segmentation network," *arXiv preprint arXiv:1902.04502*, 2019.
- [19] G. Gao, J. Yang, X.-Y. Jing, F. Shen, W. Yang, and D. Yue, "Learning robust and discriminative low-rank representations for face recognition with occlusion," *Pattern Recogn.*, vol. 66, pp. 129–143, 2017.
- [20] G. Gao, Y. Yu, J. Xie, J. Yang, M. Yang, and J. Zhang, "Constructing multilayer locality-constrained matrix regression framework for noise robust face super-resolution," *Pattern Recogn.*, vol. 110, p. 107539, 2021.
- [21] G. Gao, Y. Yu, J. Yang, G.-J. Qi, and M. Yang, "Hierarchical deep cnn feature set-based representation learning for robust cross-resolution face recognition," *arXiv preprint arXiv:2103.13851*, 2021.
- [22] X. Zhang, Z. Chen, Q. J. Wu, L. Cai, D. Lu, and X. Li, "Fast semantic segmentation for scene perception," *IEEE Trans. Ind. Informat.*, vol. 15, no. 2, pp. 1183–1192, 2019.
- [23] T. Wu, S. Tang, R. Zhang, J. Cao, and Y. Zhang, "Cgnet: A light-weight context guided network for semantic segmentation," *IEEE Trans. Image Process.*, vol. 30, pp. 1169–1179, 2020.
- [24] M. Yang, K. Yu, C. Zhang, Z. Li, and K. Yang, "Denseaspp for semantic segmentation in street scenes," in *Proc. CVPR*, 2018, pp. 3684–3692.
- [25] L.-C. Chen, G. Papandreou, I. Kokkinos, K. Murphy, and A. L. Yuille, "Deeplab: Semantic image segmentation with deep convolutional nets, atrous convolution, and fully connected crfs," *IEEE Trans. Pattern Anal. Mach. Intell.*, vol. 40, no. 4, pp. 834–848, 2017.
- [26] L.-C. Chen, G. Papandreou, F. Schroff, and H. Adam, "Rethinking atrous convolution for semantic image segmentation," *arXiv preprint arXiv:1706.05587*, 2017.
- [27] C. Yu, J. Wang, C. Peng, C. Gao, G. Yu, and N. Sang, "Learning a discriminative feature network for semantic segmentation," in *Proc. CVPR*, 2018, pp. 1857–1866.
- [28] E. Romera, J. M. Alvarez, L. M. Bergasa, and R. Arroyo, "Erfnet: Efficient residual factorized convnet for real-time semantic segmentation," *IEEE Trans. Intell. Transp. Syst.*, vol. 19, no. 1, pp. 263–272, 2017.
- [29] E. Shelhamer, J. Long, and T. Darrell, "Fully convolutional networks for semantic segmentation," *IEEE Trans. Pattern Anal. Mach. Intell.*, vol. 39, no. 4, pp. 640–651, 2017.
- [30] Y. Wang, Q. Zhou, J. Liu, J. Xiong, G. Gao, X. Wu, and L. J. Latecki, "Lednet: A lightweight encoder-decoder network for real-time semantic segmentation," in *Proc. ICIP*, 2019, pp. 1860–1864.
- [31] G. Li, I. Yun, J. Kim, and J. Kim, "Dabnet: Depth-wise asymmetric bottleneck for real-time semantic segmentation," *arXiv preprint arXiv:1907.11357*, 2019.
- [32] M. Sandler, A. Howard, M. Zhu, A. Zhmoginov, and L.-C. Chen, "Mobilenetv2: Inverted residuals and linear bottlenecks," in *Proc. CVPR*, 2018, pp. 4510–4520.
- [33] S. Ioffe and C. Szegedy, "Batch normalization: Accelerating deep network training by reducing internal covariate shift," in *Proc. ICML*, 2015, pp. 448–456.
- [34] V. Nair and G. E. Hinton, "Rectified linear units improve restricted boltzmann machines," in *Proc. ICML*, 2010, pp. 1–8.
- [35] C. Szegedy, V. Vanhoucke, S. Ioffe, J. Shlens, and Z. Wojna, "Rethinking the inception architecture for computer vision," in *Proc. CVPR*, 2016, pp. 2818–2826.
- [36] A. Howard, M. Sandler, G. Chu, L.-C. Chen, B. Chen, M. Tan, W. Wang, Y. Zhu, R. Pang, V. Vasudevan *et al.*, "Searching for mobilenetv3," in *Proc. ICCV*, 2019, pp. 1314–1324.
- [37] X. Zhang, X. Zhou, M. Lin, and J. Sun, "Shufflenet: An extremely efficient convolutional neural network for mobile devices," in *Proc. CVPR*, 2018, pp. 6848–6856.
- [38] N. Ma, X. Zhang, H.-T. Zheng, and J. Sun, "Shufflenet v2: Practical guidelines for efficient cnn architecture design," in *Proc. ECCV*, 2018, pp. 116–131.
- [39] A. Krizhevsky, I. Sutskever, and G. E. Hinton, "Imagenet classification with deep convolutional neural networks," in *Proc. NeurIPS*, 2012, pp. 1097–1105.
- [40] S. Woo, J. Park, J.-Y. Lee, and I. So Kweon, "Cbam: Convolutional block attention module," in *Proc. ECCV*, 2018, pp. 3–19.
- [41] X. Wang, R. Girshick, A. Gupta, and K. He, "Non-local neural networks," in *Proc. CVPR*, 2018, pp. 7794–7803.
- [42] J. Fu, J. Liu, H. Tian, Y. Li, Y. Bao, Z. Fang, and H. Lu, "Dual attention network for scene segmentation," in *Proc. CVPR*, 2019, pp. 3146–3154.
- [43] Z. Huang, X. Wang, L. Huang, C. Huang, Y. Wei, and W. Liu, "Ccnnet: Criss-cross attention for semantic segmentation," in *Proc. ICCV*, 2019, pp. 603–612.
- [44] Q. Hou, D. Zhou, and J. Feng, "Coordinate attention for efficient mobile network design," *arXiv preprint arXiv:2103.02907*, 2021.
- [45] M. Trembl, J. Arjona-Medina, T. Unterthiner, R. Durgesh, F. Friedmann, P. Schuberth, A. Mayr, M. Heusel, M. Hofmarcher, M. Widrich *et al.*, "Speeding up semantic segmentation for autonomous driving," in *ML-ITS, NIPS Workshop*, vol. 2, no. 7, 2016.
- [46] Z. Yang, H. Yu, Q. Fu, W. Sun, W. Jia, M. Sun, and Z.-H. Mao, "Ndnnet: Narrow while deep network for real-time semantic segmentation," *IEEE Trans. Intell. Transp. Syst.*, p. DOI: 10.1109/TITS.2020.2987816, 2020.
- [47] S. Mehta, M. Rastegari, L. Shapiro, and H. Hajishirzi, "Espnetv2: A light-weight, power efficient, and general purpose convolutional neural network," in *Proc. CVPR*, 2019, pp. 9190–9200.
- [48] S.-Y. Lo, H.-M. Hang, S.-W. Chan, and J.-J. Lin, "Efficient dense modules of asymmetric convolution for real-time semantic segmentation," in *Proc. MMAsia*, 2019, pp. 1–6.
- [49] T. Pohlen, A. Hermans, M. Mathias, and B. Leibe, "Full-resolution residual networks for semantic segmentation in street scenes," in *Proc. CVPR*, 2017, pp. 4151–4160.

Guangwei Gao (Member, IEEE) received the Ph.D. degree in pattern recognition and intelligence systems from the Nanjing University of Science and Technology, Nanjing, in 2014. He was a Project Researcher with the National Institute of Informatics, Tokyo, Japan, in 2019. He is currently an Associate Professor with the Institute of Advanced Technology, Nanjing University of Posts and Telecommunications. His research interests include pattern recognition, and computer vision. He has served as reviewer for IEEE TNNLS/TIP/TMM/TCYB, Pattern Recognition, Neurocomputing, Pattern Recognition Letters, and AAAI/ICPR/ICIP etc.

Guoan xu received the B.S degrees in Measurement Control Technology and Instrumentation from Changshu Institute of Technology, Jiangsu, China, in 2019. He is currently pursuing the M.S. degree with the College of Automation & College of Artificial Intelligence, Nanjing University of Posts and Telecommunications. His research interests include image semantic segmentation.

Juncheng Li received the B.S. degree in Computer Science and Technology from Jiangxi Normal University, Nanchang, China, in 2016, and the Ph.D. degree in Computer Science and Technology from East China Normal University, Shanghai, China, in 2021. He is currently a Postdoctoral Fellow at the Center for Mathematical Artificial Intelligence, The Chinese University of Hong Kong. His main research interests includes image restoration, computer vision, deep learning, and medical image processing.

Yi Yu (Member, IEEE) received the Ph.D. degree in information and computer science from Nara Women's University, Japan. He is currently an Assistant Professor with the National Institute of Informatics (NII), Japan. Before joining NII, she was a Senior Research Fellow with the School of Computing, National University of Singapore. Her research covers large-scale multimedia data mining and pattern analysis, location-based mobile media service and social media analysis. She and her team received the best Paper Award from the IEEE ISM 2012, the 2nd prize in Yahoo Flickr Grand Challenge 2015, were in the top winners (out of 29 teams) from ACM SIGSPATIAL GIS Cup 2013, and the Best Paper Runner-Up in APWeb-WAIM 2017, recognized as finalist of the World's FIRST 10K Best Paper Award in ICME 2017.

Huimin Lu (Senior Member, IEEE) received the B.S. degree in electronics information science and technology from Yangzhou University in 2008, the M.S. degree in electrical engineering from the Kyushu Institute of Technology and Yangzhou University in 2011, and the Ph.D. degree in electrical engineering from the Kyushu Institute of Technology in 2014. From 2013 to 2016, he was a JSPS Research Fellow (DC2, PD, and FPD) with the Kyushu Institute of Technology. He is currently an Assistant Professor with the Kyushu

Institute of Technology and an Excellent Young Researcher of MEXT-Japan. His research interests include computer vision, robotics, artificial intelligence, and ocean observing.

Jian Yang (Member, IEEE) received the PhD degree from Nanjing University of Science and Technology (NUST), on the subject of pattern recognition and intelligence systems in 2002. In 2003, he was a postdoctoral researcher at the University of Zaragoza. From 2004 to 2006, he was a Postdoctoral Fellow at Biometrics Centre of Hong Kong Polytechnic University. From 2006 to 2007, he was a Postdoctoral Fellow at Department of Computer Science of New Jersey Institute of Technology. Now, he is a Chang-Jiang professor in the School of Computer Science and Engineering of NUST. He is the author of more than 100 scientific papers in pattern recognition and computer vision. His papers have been cited more than 4000 times in the Web of Science, and 9000 times in the Scholar Google. His research interests include pattern recognition, computer vision and machine learning. Currently, he is/was an Associate Editor of Pattern Recognition Letters, IEEE Trans. Neural Networks and Learning Systems, and Neurocomputing. He is a Fellow of IAPR.